

RESEARCH LETTER

10.1002/2015GL065937

Key Points:

- Wave scattering theory alone is not sufficient to predict attenuation of waves
- Wave energy is not conserved during wave-ice interactions
- Turbulent bores at the floes front and rear edges induce dissipation

Correspondence to:

A. Toffoli,
toffoli.alessandro@gmail.com

Citation:

Toffoli, A., L. G. Bennetts, M. H. Meylan, C. Cavaliere, A. Alberello, J. Elsnaab, and J. P. Monty (2015), Sea ice floes dissipate the energy of steep ocean waves, *Geophys. Res. Lett.*, **42**, 8547–8554, doi:10.1002/2015GL065937.

Received 26 AUG 2015

Accepted 2 OCT 2015

Accepted article online 8 OCT 2015

Published online 25 OCT 2015

Sea ice floes dissipate the energy of steep ocean waves

A. Toffoli¹, L. G. Bennetts², M. H. Meylan³, C. Cavaliere³, A. Alberello¹, J. Elsnaab⁴, and J. P. Monty⁴

¹Centre for Ocean Engineering Science and Technology, Swinburne University of Technology, Hawthorn, Victoria, Australia, ²School of Mathematical Sciences, University of Adelaide, Adelaide, South Australia, Australia, ³School of Mathematical and Physical Sciences, University of Newcastle, Callaghan, New South Wales, Australia, ⁴Department of Mechanical Engineering, University of Melbourne, Melbourne, Victoria, Australia

Abstract A laboratory experimental model of an incident ocean wave interacting with an ice floe is used to validate the canonical, solitary floe version of contemporary theoretical models of wave attenuation in the ice-covered ocean. Amplitudes of waves transmitted by the floe are presented as functions of incident wave steepness for different incident wavelengths. The model is shown to predict the transmitted amplitudes accurately for low incident steepness but to overpredict the amplitudes by an increasing amount, as the incident wave becomes steeper. The proportion of incident wave energy dissipated by the floe in the experiments is shown to correlate with the agreement between the theoretical model and the experimental data, thus implying that wave-floe interactions increasingly dissipate wave energy as the incident wave becomes steeper.

1. Introduction

Arctic sea ice is retreating in response to climate change [e.g., *Stroeve et al.*, 2014]. The emerging regions of open water, for example, in the Beaufort and Chukchi Seas, provide fetch for winds to generate large-amplitude ocean surface waves [*Francis et al.*, 2011; *Thomson and Rogers*, 2014; *Khon et al.*, 2014]. The waves penetrate deep into the ice-covered ocean and impact the ice cover [e.g., *Liu and Mollo-Christensen*, 1988]. Concomitantly, the ice cover attenuates the wave energy over distance, so that wave impacts eventually die out [e.g., *Wadhams et al.*, 1988]. The region in which waves impacts remain significant is known as the marginal ice zone (MIZ).

The most heralded impact is the ability of waves to break up large floes into floes with diameters comparable to the prevailing wavelengths. For example, *Collins et al.* [2015] report a breakup event observed from a vessel in the Barents Sea in 2010, with wave motion inferred from an onboard GPS. Further, *Prinsenbergh and Peterson* [2011] and *Asplin et al.* [2012] report wave-induced breakup 250 km into the Beaufort Sea in 2009. The smaller floes melt more rapidly than larger floes, which has led to the hypothesis that waves are accelerating Arctic ice retreat [e.g., *Squire*, 2011; *Thomson and Rogers*, 2014].

Antarctic sea ice is exposed to intense storm waves generated in the Southern Ocean. Consequently, the Antarctic ice pack is encircled by a MIZ up to hundreds of kilometers in width. *Kohout et al.* [2014] provide evidence that trends in the contraction and expansion of the Antarctic sea ice edge are correlated to trends in the increase and decrease of the local significant wave height, respectively, over the 1997–2009 period. They conjecture that wave-induced breakup is responsible for this relationship and report a breakup event over 300 km into the Antarctic MIZ during the Sea Ice Physics and Ecosystem Experiment 2012 (SIPEX-II), which *Kohout et al.* [2015] analyze.

The changes to the Arctic and the new findings are driving integration of wave-ice interactions into large-scale numerical forecasting and climate models. Theoretical models of wave attenuation in the ice-covered ocean undergird the integration. Following numerous findings that ice cover acts as a low-pass filter, i.e., it attenuates short-period waves more rapidly than long-period waves [e.g., *Squire and Moore*, 1980], the models predict attenuation rates as a function of wave period.

Attenuation models are conventionally based on wave scattering theory and linearization with respect to wave steepness (see the review of *Squire* [2007]). Scattering redistributes wave energy across the directional spectrum without net energy loss. Each floe reflects a proportion of the incident wave energy, and the cumulative effect is attenuation over distance.

Linear attenuation models based on dissipation have also been proposed, i.e., wave energy is removed from the wave-ice system to produce attenuation, as opposed to scattering of wave energy producing the attenuation. The dissipative mechanisms modeled include hysteresis [Wadhams, 1973], floe-floe collisions [Shen and Squire, 1998], drag at the ice-ocean interface [Kohout et al., 2011], and viscosity of unspecified source [Keller, 1998; Wang and Shen, 2010; Mosig et al., 2015].

Doble and Bidlot [2013] integrated the scattering attenuation model of Kohout and Meylan [2008] and drag dissipation model of Kohout et al. [2011] into the WAM wave model. They show that model predictions of significant wave heights and wave periods are generally consistent with measurements provided by a wave buoy deployed in the Antarctic MIZ. However, they show that the model consistently underpredicts attenuation of the slightly shorter period components of the wave spectrum (with respect to the peak).

In a series of papers, Dumont et al. [2011] and Williams et al. [2012, 2013a, 2013b] developed a coupled attenuation and breakup model and integrated it into a regional version of the HYCOM ice/ocean model. They used the combined scattering attenuation and parameterized dissipation attenuation model of Bennetts and Squire [2012]. They show that model predictions of breakup are most sensitive to the attenuation rate. Therefore, accurate predictions of breakup require further development of attenuation models.

More recently, first Zhang et al. [2015] and subsequently Horvat and Tziperman [2015] proposed theoretical/numerical models of the evolution of the MIZ ice floe distribution in response to oceanic and atmospheric forcing. They identify attenuation and wave-induced breakup as key model components and incorporate these processes using the theories outlined in Dumont et al. [2011] and Williams et al. [2013a, 2013b].

Meylan et al. [2014] calculated attenuation rates from measurements provided by an array of five wave sensors in the Antarctic MIZ during SIPEX-II. They show that attenuation rates increase as wave amplitudes increase for short-period components of the wave spectrum. The linear scattering attenuation model cannot predict this behavior and therefore underpredicts attenuation of large-amplitude waves. The sources of the amplitude dependence are not yet known.

In situ measurements of attenuation rates provide some validation of attenuation models [e.g., Kohout and Meylan, 2008; Bennetts et al., 2010]. However, they do not indicate the processes responsible for disagreements, due to the coarse spatial resolution of the measurements and the lack of accompanying information on the properties of the ice cover. Methods to measure attenuation via satellite images are only now being developed [Ardhuin et al., 2015].

To complement the field measurements, laboratory experimental models are now being used to gain insight into the attenuation process. Bennetts et al. [2015] analyzed wave fields transmitted by solitary floes, modeled by thin square plastic plates, in a large wave basin. Two different plastics were tested, with different densities and Young's moduli and three different thicknesses. The model floes were subjected to regular incident waves for a range of wave periods and steepnesses below the wave-breaking limit. They showed, in particular, that the transmitted wave fields are regular for low-steepness incident waves but become highly irregular for steeper incident waves. This implies that both the linear scattering and viscous models will be inaccurate beyond a certain steepness limit. However, their measurements were unable to show whether the wave-floe interactions dissipated wave energy, due to the three-dimensional nature of the tests, i.e., waves being scattered across the directional spectrum.

In this letter, an essentially two-dimensional experimental model of a regular incident wave interacting with a floe is used to validate the canonical, solitary floe version of the scattering attenuation model for low incident steepnesses and indicate its limit of validity with respect to steepness. Attenuation is inferred from the transmitted wave field. Dissipation is inferred from the sum of the reflected and transmitted energies.

2. Experimental Model

The experimental model was implemented in the Extreme Wind-Wave Flume, University of Melbourne, Australia. Figure 1 (left) shows a schematic plan view of the flume and experimental setup. The flume is 60m long and 1.8m wide and was filled with fresh water of density $\rho \approx 1000 \text{ kgm}^{-3}$, up to a depth of $H = 0.8 \text{ m}$. It is equipped with a wave maker at its right-hand end and a beach at its left-hand end.

The wave maker generated plane (regular) incident waves. Three incident wave periods were tested: $T = 0.8 \text{ s}$, 0.9 s , and 1 s , which correspond to wavelengths $\lambda = 1.00 \text{ m}$, 1.26 m , and 1.56 m , respectively.

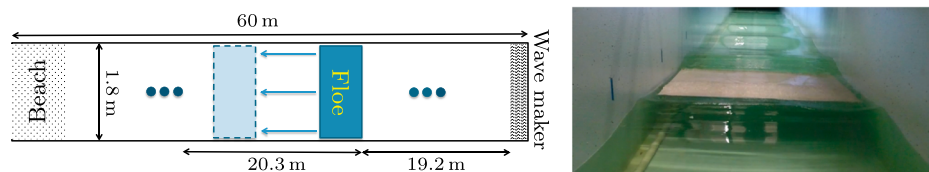


Figure 1. (left) A schematic plan view of experimental setup (not to scale). Dots represent wave gauge locations. (right) Photo of model floe during a test, facing toward the beach.

Six target incident amplitudes, a_{inc} , were tested for each period. The amplitudes were selected to produce target wave steepnesses $ka_{inc} = 0.04, 0.06, 0.08, 0.1, 0.12,$ and 0.14 , where $k = 2\pi/\lambda$ is the wave number. This steepness range covers gently sloping to storm-like waves but does not reach the breaking onset ($ka > 0.33$) [Babanin et al., 2007].

Side bands were not applied to the input plane waves. Therefore, even if background noise can act as a perturbation, the flume is not long enough for modulational (Benjamin-Feir) instability to develop [see, e.g., Tulin and Waseda, 1999; Toffoli et al., 2013]. Nonlinear wave dynamics and consequent generation of wave breaking is excluded.

A rectangular, polypropylene plastic plate was used as a model floe. It was $l = 1$ m long, 1.7 m wide, and $h = 10$ mm thick. Figure 1 (right) shows a photo of the model floe during a test. The polypropylene plate has manufacturer-specified Young's modulus $E = 1.6$ GPa and density $\rho_f = 905$ kg m⁻³. The model floe has density and, hence, freeboard, comparable to sea ice. The Young's modulus is multiplied by the geometric scaling factor to obtain its equivalent field value. Measurements of the Young's modulus of sea ice are between 1 GPa and 10 GPa [Timco and Weeks, 2010]. Therefore, the model floe is more rigid than field scale floes for scaling factors greater than approximately 6.25.

The floe was deployed 19.2 m from the wave maker. It oscillates in response to the waves, in surge, heave, and pitch, along with some elastic responses. No mooring was applied to the floe. Therefore, it was free to drift in response to the incident wave except for occasional collisions with the side walls. No anomalies were detected in the measurements due to the collisions. The drift velocity was calculated using videos of the floe during the tests and markers on the flume walls. It depended on the incident wave period and steepness. Its smallest value was 0.04 m s⁻¹, which occurred for the shortest period and lowest steepness, $T = 0.8$ s and $ka = 0.04$. Its largest value was 0.20 m s⁻¹, which occurred for the longest period and highest steepness, $T = 1.0$ s and $ka = 0.14$. In all cases, the drift velocity was greater than Stokes drift velocity, which is consistent with the findings of Huang and Law [2013]. (See also Christensen and Weber [2005], who show that Weber's [1987] theoretical model of drift of a body much longer than the waves accurately predicts Law's [1999] laboratory experimental measurements of the drift velocities of thin, rectangular polypropylene sheets twice as long as the incident wavelength or greater and that these velocities are several times greater than the corresponding Stokes drift velocities.)

A line of three capacitance wave gauges on the beach side of the floe recorded the surface elevation of the transmitted wave field, η_{tra} , at a frequency of 1000 Hz. The gauges were deployed far enough from the initial location of the floe not to disrupt its free drift and far enough from the beach to maximize the recording duration before they were contaminated by waves reflected by the beach. A corresponding line of gauges on the wave maker side of the floe recorded the surface elevation of the incident plus the reflected wave field, $\eta_{inc+ref}$. The schematic in Figure 1 shows the gauge locations.

For each test, the wave maker ran from $t = 0$ to $t = 90$ s. The surface elevation time series were restricted to a sufficiently small time frame to exclude contamination of residual reflection from the beach. The time windows were $t \leq 64$ s, $t \leq 57$ s, and $t \leq 51$ s, for wave periods of $T = 0.8$ s, $T = 0.9$ s, and $T = 1.0$ s, respectively. Records were only analyzed after the initial transients in the wave field had passed, which was after 21 s, 19 s, and 18 s for the probes on the wave maker side and 37 s, 34 s, and 31 s for the probes on the beach side, for the wave periods $T = 0.8$ s, $T = 0.9$ s, and $T = 1.0$ s, respectively. Each test was repeated three times to increase the statistical significance of the results. Further, each test was conducted once without the floe to provide benchmark surface elevation measurements of the incident waves, η_{inc} , at each gauge location.

3. Theoretical Scattering Model

The two-dimensional version of the scattering model is used to model the experiments. It considers motions in a cross section parallel to the side walls of the tank and away from the walls, assuming that interactions between adjacent cross sections are negligible. The Cartesian coordinate (x, z) denotes locations in a given cross section. Here x defines the horizontal location, which points in the direction of the incident wave and has its origin set to coincide with the front edge of the floe at rest. The coordinate z defines the vertical location. It points upward and has its origin set to coincide with the water surface at rest.

The model is based on combined potential flow and thin-plate theories. It has been the cornerstone of wave-ice interaction models for over three decades, e.g., from *Wadhams et al.* [1988] to *Kohout and Meylan* [2008]. Potential flow theory assumes that the water is homogeneous, inviscid, incompressible, and in irrotational motion. It follows that the water velocity field can be defined as the gradient of a scalar velocity potential, denoted $\Phi(x, z, t)$. The surface elevation is calculated from the velocity potential via $\eta(x, t) = \Phi_t(x, z = \eta, t)/g$, where $g \approx 9.81 \text{ ms}^{-2}$ is gravitational acceleration. Thin-plate theory defines the deformation of the floe in terms of the vertical displacements of its lower surface, denoted $z = -d + w(x, t)$, where $d = \rho_f h / \rho$ is the Archimedean draft of the floe. The horizontal location of the floe's center of mass is denoted by $u(t)$.

Wave steepnesses are assumed to be sufficiently small that linear theory is valid. Thus, the water-floe system oscillates at the frequency of the incident wave. The velocity potential, displacement function, and lateral motion are expressed as

$$\Phi(x, z, t) = \text{Re} \{ (g/i\omega)\phi(x, z)e^{-i\omega t} \}, \quad w(x, t) = \text{Re} \{ \zeta(x)e^{-i\omega t} \}, \quad (1)$$

$$\text{and} \quad u(t) = \text{Re} \{ \xi e^{-i\omega t} \}, \quad (2)$$

where $\omega = 2\pi/T$ is angular frequency and ϕ, ζ and ξ are complex valued.

The (reduced) velocity potential, ϕ , satisfies Laplace's equation in the water domain, an impermeable floor condition, and the linearized free-surface condition at points not covered by the floe, i.e.,

$$\phi_{xx} + \phi_{zz} = 0 \quad \text{for} \quad (x, z) \in \Omega, \quad \phi_z = 0 \quad \text{for} \quad z = -H, \quad (3)$$

$$\text{and} \quad \phi_z = \sigma\phi \quad \text{for} \quad x \notin (0, l) \quad \text{and} \quad z = 0, \quad (4)$$

respectively, where $\sigma = \omega^2/g$ is a frequency parameter. The water and floe motions are coupled by dynamic and kinematic conditions applied at the wetted surface of the floe at rest. The conditions in the horizontal direction are

$$\phi_x = \sigma\xi \quad \text{for} \quad x = 0, l \quad \text{and} \quad z \in (-d, 0), \quad \text{and} \quad -\sigma h l \xi = \int_{-d}^0 [\phi]_{x=0}' dz. \quad (5)$$

The conditions in the vertical direction are

$$\phi_z = \sigma\zeta \quad \text{and} \quad (1 - \sigma d)\zeta + F\zeta'''' = \phi \quad \text{for} \quad x \in (0, l) \quad \text{and} \quad z = -d, \quad (6)$$

where $F = Eh^3 / \{12\rho g(1 - \nu^2)\}$ is a scaled flexural rigidity of the floe and $\nu = 0.4$ is a representative value of Poisson's ratio for polypropylene. An eigenfunction matching method, similar to that outlined by *Montiel et al.* [2012], is used to solve the above boundary value problem for ϕ, ζ , and ξ .

On the incident wave side of the floe, far enough away from the floe that the exponentially decaying local motions have died out, the wave field is the sum of the incident wave plus a reflected wave. On the opposite side of the floe, far enough away from the floe, the wave field is composed of a transmitted wave only. The incident, reflected, and transmitted wave elevations for the linear problem are defined as

$$\eta_{\text{inc}} = a_{\text{inc}} \cos(kx - \omega t), \quad \eta_{\text{ref}} = a_{\text{ref}} \cos(kx - \omega t + \varphi_{\text{ref}}), \quad (7)$$

$$\text{and} \quad \eta_{\text{tra}} = a_{\text{tra}} \cos(kx - \omega t + \varphi_{\text{tra}}), \quad (8)$$

respectively, where a_{ref} and a_{tra} are the reflected and transmitted amplitudes and φ_{ref} and φ_{tra} are phases.

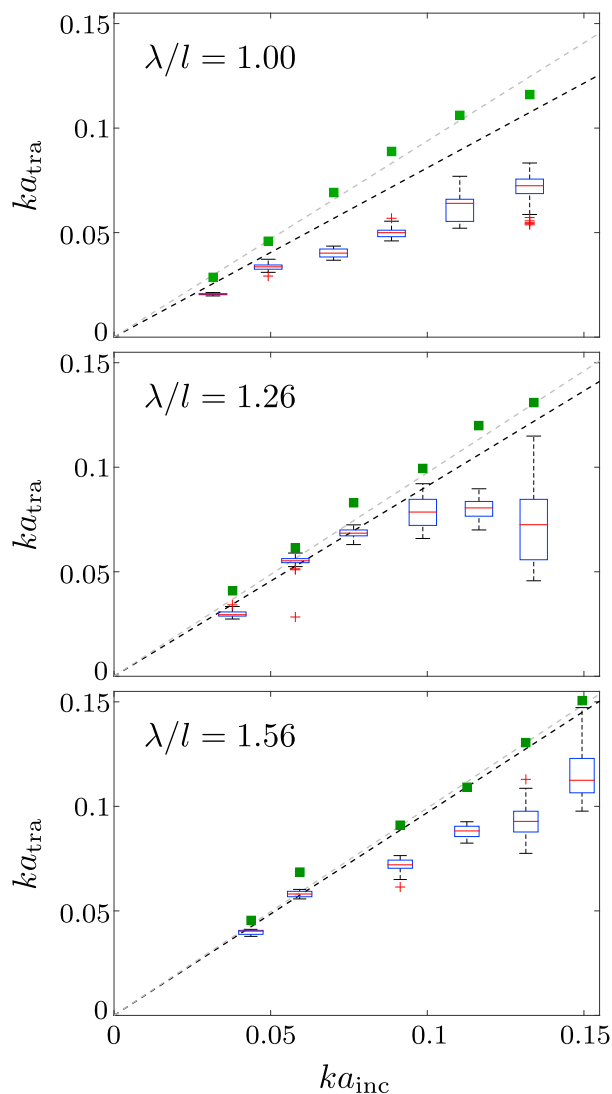


Figure 2. Experimental measurements of transmitted amplitudes, represented as box-and-whisker plots of nondimensional transmitted amplitudes as functions of incident steepness. The three panels represent results for different incident wavelengths, λ , which are nondimensionalized with respect to the floe length, l . Green squares denote median nondimensional transmitted amplitudes from the benchmark (no floe) tests. Broken lines show theoretical model predictions. Black lines use the Young's modulus of the polypropylene plastic, and grey lines use the Young's modulus of sea ice at basin scale.

The green squares in the plots denote the nondimensional amplitudes on the beach side from the benchmark tests (no floe). They show that the amplitudes on the beach side (transmitted fields) are approximately equal to the amplitudes on the wave maker side (incident fields). The test using the shortest incident wavelength and highest steepness is the only notable exception. Here the transmitted amplitude is slightly less than incident amplitude, which is attributed to viscous losses in the water. The benchmark test results confirm that it is the presence of the floe that causes transmitted wave amplitudes to be smaller than the incident amplitudes.

Theoretical model predictions are overlaid on the plots, as black broken lines. The model predicts the linear relationship $ka_{tra} = \mathcal{T} \times ka_{inc}$. The value of \mathcal{T} changes between the panels. It increases monotonically from 0.81 for $\lambda/l = 1.00$ to 0.97 for $\lambda/l = 1.56$, which is approximately full transmission. For reference, the model predictions for a Young's modulus $E = 6/40$ GPa are shown as grey lines. Here 6 GPa is the standard value of Young's modulus used in wave-ice interaction models [Squire, 2007], and 40 is the appropriate geometric

The model conserves wave energy. Thus, the proportion of incident wave energy dissipated is $\mathcal{D} \equiv 1 - \mathcal{R} - \mathcal{T} = 0$, where $\mathcal{R} = |a_{ref}/a_{inc}|^2$ and $\mathcal{T} = |a_{tra}/a_{inc}|^2$ are the proportions of reflected and transmitted energies, respectively.

4. Results and Analysis

Individual transmitted wave heights were calculated by applying a zero-crossing analysis to time series provided by the three wave gauges on the beach side of the floe [e.g., Emery and Thomson, 2001]. Both down-crossing and up-crossing heights were calculated. The series were first low- and high-pass filtered to remove contaminating components greater than 5.5 times and smaller than 0.35 times the dominant frequency. The filtered components contribute less than 0.1% to the total transmitted energy. Transmitted amplitudes, a_{tra} , were calculated as half of their corresponding wave heights.

Figure 2 shows box-and-whisker plots of the nondimensional transmitted amplitudes, ka_{tra} , as functions of incident steepness, ka_{inc} , where the incident amplitude, a_{inc} , represents the mean amplitude measured by the three gauges closest to the wave maker in the benchmark tests. The limits of the boxes represent the 25th and 75th percentiles of the samples. The horizontal red lines represent the medians. The whiskers extend to the most extreme data points not more than 1.5 times the height of the box away from the box. Observations beyond the whiskers are represented by pluses and are considered outliers. The different panels represent the results for different incident wavelengths, nondimensionalized with respect to the floe length.

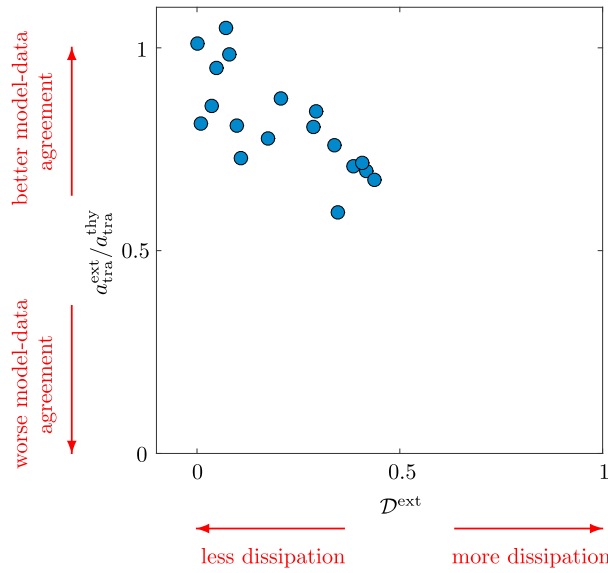


Figure 3. Scattered energy proportion for individual tests versus deviation of experimentally measured transmitted amplitudes from theoretical model prediction.

$\lambda/l = 1.26$ but only occurs for the three highest steepnesses. The data for the highest steepness indicate a tendency for transmitted steepnesses to decrease with increasing steepness. However, the data are widely spread. For example, the box covers over 19% of the nondimensional amplitude range displayed. This implies highly irregular transmitted wave fields, which a single amplitude is unable to quantify. For $\lambda/l = 1.00$ the model prediction does not lie within the box or whiskers for any incident steepnesses tested. Nevertheless, the model is reasonably close to the experimental measurements for the two lowest incident steepnesses.

Figure 2 suggests that wave-floe interactions dissipate an increasing proportion of the incident wave energy, as the incident waves become steeper and, hence, the model becomes less accurate. Figure 3 validates this inference. It shows the model-data agreement versus the proportion of wave energy dissipated in the experiments, $D^{ext} = 1 - \mathcal{R}^{ext} - \mathcal{T}^{ext}$. The reflected and transmitted energy proportions are calculated from the experimental data via

$$\mathcal{R}^{ext} = \left\langle \frac{|m_0[\eta_{inc+ref}] - m_0[\eta_{inc}]|}{m_0[\eta_{inc}]} \right\rangle \quad \text{and} \quad \mathcal{T}^{ext} = \left\langle \frac{m_0[\eta_{tra}]}{m_0[\eta_{inc}]} \right\rangle, \quad (9)$$

$$\text{where} \quad m_0[\eta] = \int_0^\infty E(f)df \quad (10)$$

is the spectral variance and the angled brackets denote the mean with respect to the reflected or transmitted wave gauges, as appropriate. The model-data agreement is represented by the quotient $a_{tra}^{ext}/a_{tra}^{thy}$, where a_{tra}^{ext} is the median experimental measurement of the transmitted amplitude and a_{tra}^{thy} is the corresponding theoretical model prediction.

A subset of the data points are clustered close to $(D^{ext}, a_{tra}^{ext}/a_{tra}^{thy}) = (0, 1)$. This indicates that energy is conserved when the model and data agree, i.e., when the incident waves have low steepness. Although some scatter is evident, the data show a negative correlation between the model-data agreement and the dissipated energy. This indicates that the overpredictions of the transmitted amplitudes are predominantly due to unmodeled dissipative processes.

The clearest source of wave energy dissipation during the experiments was due to waves becoming turbulent and breaking on the upper surface of the floe, noting that waves were not steep enough to break in the water surrounding the floe. Incident waves wash over the upper surface of the floe, due to its small freeboard. Overwash was negligible for low-steepness incident waves. However, for steep incident waves, the overwash became deep and energetic. Turbulent bores were generated at the floe’s front and rear edges. When these

scaling factor for a typical floe thickness in the Antarctic winter MIZ [Toyota et al., 2011]. The impact of the reduced rigidity on transmission is modest and decreases as the incident wave becomes longer, as long waves predominantly excite rigid motions [Meylan et al., 2015].

For the longest incident wave, $\lambda/l = 1.56$, and the two lowest incident steepnesses, the model and data agree—the model predictions lie in the narrow boxes. As the incident steepness increases, the experimental measurements drop below the model predictions. Moreover, the boxes and whiskers cover larger ranges for steeper incident waves, which is a result of the transmitted waves becoming irregular for steep incident waves, as noted by Bennetts et al. [2015].

Similar trends occur for the two shorter incident waves. The deviation of the data from the predictions is strongest for

bores collided, the surface profile became steep enough to break. Theoretical models of wave energy dissipation due to overwash do not yet exist, although *Skene et al.* [2015] recently modeled the onset and depth of overwash.

5. Summary

An experimental model of ocean wave interactions with an ice floe was used to validate the solitary floe version of the quintessential theoretical model of wave attenuation in the ice-covered ocean. The experimental model was implemented in a wave flume, using a thin plastic plate to model the floe. Wave gauges recorded the incident, reflected, and transmitted wave fields.

The theoretical model was shown to predict transmitted wave amplitudes accurately for gently sloping incident waves. However, it increasingly overpredicted transmitted amplitudes, as the incident waves became steeper and increasingly storm-like. The loss of agreement was shown to correlate with wave energy being dissipated by the wave-floe interactions in the experiments.

Acknowledgments

The Universities of Melbourne and Newcastle funded the experiments. The Australian Research Council funds an early-career fellowship for L.G.B. (DE130101571) and a midcareer fellowship for J.P.M. (FT120100409). The Australian Antarctic Science Program provides support for L.G.B. (project 4123). M.H.M. acknowledges support from the U.S. Office of Naval Research (project N00014-13-1-0290). The experimental data used for this study may be obtained from the corresponding author (email: toffoli.alessandro@gmail.com).

References

- Ardhuin, F., F. Collard, B. Chapron, F. Girard-Ardhuin, G. Guitton, A. Mouche, and J. Stopa (2015), Estimates of ocean wave heights and attenuation in sea ice using the SAR wave mode on Sentinel-1A, *Geophys. Res. Lett.*, *42*, 2317–2325, doi:10.1002/2014GL062940.
- Asplin, M. G., R. Galley, D. G. Barber, and S. Prinsenberg (2012), Fracture of summer perennial sea ice by ocean swell as a result of Arctic storms, *J. Geophys. Res.*, *117*, C06025, doi:10.1029/2011JC007221.
- Babanin, A. V., D. Chalikov, I. Young, and I. Savelyev (2007), Predicting the breaking onset of surface water waves, *Geophys. Res. Lett.*, *34*, L07605, doi:10.1029/2006GL029135.
- Bennetts, L. G., and V. A. Squire (2012), On the calculation of an attenuation coefficient for transects of ice-covered ocean, *Proc. R. Soc. Lond. A*, *468*(2137), 136–162.
- Bennetts, L. G., M. A. Peter, V. A. Squire, and M. H. Meylan (2010), A three-dimensional model of wave attenuation in the marginal ice zone, *J. Geophys. Res.*, *115*, C12043, doi:10.1029/2009JC005982.
- Bennetts, L. G., A. Alberello, M. H. Meylan, C. Cavaliere, A. V. Babanin, and A. Toffoli (2015), An idealised experimental model of ocean surface wave transmission by an ice floe, *Ocean Model.*, doi:10.1016/j.ocemod.2015.03.001, in press.
- Collins, C. O., W. E. Rogers, A. Marchenko, and A. V. Babanin (2015), In situ measurements of an energetic wave event in the Arctic marginal ice zone, *Geophys. Res. Lett.*, *42*, 1863–1870, doi:10.1002/2015GL063063.
- Christensen, K. H., and J. E. Weber (2005), Wave-induced drift of large floating sheets, *Environ. Fluid Mech.*, *5*, 495–505, doi:10.1007/s10652-005-1052-8.
- Doble, M. J., and J.-R. Bidlot (2013), Wavebuoy measurements at the Antarctic sea ice edge compared with an enhanced ECMWF WAM: Progress towards global waves-in-ice modeling, *Ocean Model.*, *70*, 166–173.
- Dumont, D., A. L. Kohout, and L. Bertino (2011), A wave-based model for the marginal ice zone including a floe breaking parameterization, *J. Geophys. Res.*, *116*, C04001, doi:10.1029/2010JC006682.
- Emery, W., and R. Thomson (2001), *Data Analysis Methods in Physical Oceanography, Advanced Series on Ocean Engineering*, Elsevier Science B.V., Amsterdam.
- Francis, O. P., G. G. Panteleev, and D. E. Atkinson (2011), Ocean wave conditions in the Chukchi sea from satellite and in situ observations, *Geophys. Res. Lett.*, *38*, L24610, doi:10.1029/2011GL049839.
- Horvat, C., and E. Tziperman (2015), A prognostic model of the sea ice floe size and thickness distribution, *Cryosphere Discuss.*, *9*, 2955–2997.
- Huang, G., and A. W.-K. Law (2013), Wave-induced drift of large floating objects in regular waves, *J. Waterway, Port, Coastal, Ocean Eng.*, *139*(6), 535–542, doi:10.1061/(ASCE)WW.1943-5460.0000207.
- Keller, J. B. (1998), Gravity waves on ice covered water, *J. Geophys. Res.*, *103*, 7663–7669, doi:10.1029/97JC02966.
- Khon, V. C., I. I. Mokhov, F. A. Pogarskiy, A. Babanin, K. Dethloff, A. Rinke, and H. Matthes (2014), Wave heights in the 21st century Arctic Ocean simulated with a regional climate model, *Geophys. Res. Lett.*, *41*, 2956–2961, doi:10.1002/2014GL059847.
- Kohout, A. L., and M. H. Meylan (2008), An elastic plate model for wave attenuation and ice floe breaking in the marginal ice zone, *J. Geophys. Res.*, *113*, C09016, doi:10.1029/2007JC004434.
- Kohout, A. L., M. H. Meylan, and D. R. Plew (2011), Wave attenuation in a marginal ice zone due to the bottom roughness of ice floes, *Ann. Glaciol.*, *52*(57), 118–122, doi:10.3189/172756411795931525.
- Kohout, A. L., M. J. M. Williams, S. M. Dean, and M. H. Meylan (2014), Storm-induced sea ice breakup and the implications for ice extent, *Nature*, 604–607.
- Kohout, A. L., M. J. M. Williams, T. Toyota, J. Lieser, and J. Hutchings (2015), In situ observations of wave-induced sea ice breakup, *Deep Sea Res. Part II*, doi:10.1016/j.dsr2.2015.06.010, in press.
- Law, A. W. K. (1999), Wave-induced surface drift of an inextensible thin film, *Ocean Engng.*, *26*(11), 1145–1168.
- Liu, A. K., and E. Mollo-Christensen (1988), Wave propagation in a solid ice pack, *J. Phys. Oceanogr.*, *18*(11), 1702–1712.
- Meylan, M. H., L. G. Bennetts, and A. L. Kohout (2014), In situ measurements and analysis of ocean waves in the Antarctic marginal ice zone, *Geophys. Res. Lett.*, *41*, 5046–5051, doi:10.1002/2014GL060809.
- Meylan, M. H., L. G. Bennetts, A. Alberello, C. Cavaliere, and A. Toffoli (2015), Experimental and theoretical models of wave-induced flexure of a sea ice floe, *Phys. Fluids*, *27*, 41704, doi:10.1063/1.4916573.
- Montiel, F., L. G. Bennetts, and V. A. Squire (2012), The transient response of floating elastic plates to wavemaker forcing in two dimensions, *J. Fluids Struct.*, *28*, 416–433.
- Mosig, J. E. M., F. Montiel, and V. A. Squire (2015), Comparison of viscoelastic-type models for ocean wave attenuation in ice-covered seas, *J. Geophys. Res. Oceans*, *120*, doi:10.1002/2015JC010881.
- Prinsenberg, S. J., and I. K. Peterson (2011), Observing regional-scale pack-ice decay processes with helicopter-borne sensors and moored upward-looking sonars, *Ann. Glaciol.*, *52*, 35–42.

- Shen, H. H., and V. A. Squire (1998), Wave damping in compact pancake ice fields due to interactions between pancakes, in *Antarctic Sea Ice: Physical Processes, Interactions and Variability*, AGU Antarctic Res. Ser. 74, edited by M. O. Jeffries, pp. 325–342, AGU, Washington, D. C.
- Skene, D. M., L. G. Bennetts, M. H. Meylan, and A. Toffoli (2015), Modelling water wave overwash of a thin floating plate, *J. Fluid Mech.*, *777*, R3, doi:10.1017/jfm.2015.378.
- Squire, V. A. (2007), Of ocean waves and sea-ice revisited, *Cold Reg. Sci. Technol.*, *49*, 110–133.
- Squire, V. A. (2011), Past, present and impending hydroelastic challenges in the polar and subpolar seas, *Phil. Trans. R. Soc. Lond. A*, *369*, 2813–2831.
- Squire, V. A., and S. C. Moore (1980), Direct measurement of the attenuation of ocean waves by pack ice, *Nature*, *283*, 365–368.
- Stroeve, J., T. Markus, L. Boisvert, J. Miller, and A. Barrett (2014), Changes in Arctic melt season and implications for sea ice loss, *Geophys. Res. Lett.*, *41*, 1216–1225, doi:10.1002/2013GL058951.
- Thomson, J., and W. E. Rogers (2014), Swell and sea in the emerging Arctic Ocean, *Geophys. Res. Lett.*, *41*, 3136–3140, doi:10.1002/2014GL059983.
- Timco, G. W., and W. F. Weeks (2010), A review of the engineering properties of sea ice, *Cold Reg. Sci. Technol.*, *60*, 107–129.
- Toffoli, A., T. Waseda, H. Houtani, T. Kinoshita, K. Collins, D. Proment, and M. Onorato (2013), Excitation of rogue waves in a variable medium: An experimental study on the interaction of water waves and currents, *Phys. Rev. E*, *87*, 051201(R), doi:10.1103/PhysRevE.87.051201.
- Toyota, T., C. Haas, and T. Tamura (2011), Size distribution and shape properties of relatively small sea-ice floes in the Antarctic marginal ice zone in late winter, *Deep Sea Res. Part II*, *58*(9–10), 1182–1193.
- Tulin, M. P., and T. Waseda (1999), Laboratory observation of wave group evolution, including breaking effects, *J. Fluid Mech.*, *378*, 197–232.
- Wadhams, P. (1973), Attenuation of swell by sea ice, *J. Geophys. Res.*, *78*(18), 3552–3565.
- Wadhams, P., V. A. Squire, D. J. Goodman, A. M. Cowan, and S. C. Moore (1988), The attenuation rates of ocean waves in the marginal ice zone, *J. Geophys. Res.*, *93*(C6), 6799–6818.
- Wang, R., and H. Shen (2010), Gravity waves propagating into an ice-covered ocean: A viscoelastic model, *J. Geophys. Res.*, *115*, C06024, doi:10.1029/2009JC005591.
- Weber, J. E. (1987), Wave attenuation and wave drift in the marginal ice zone, *J. Phys. Oceanogr.*, *17*(12), 2351–2361.
- Williams, T. D., L. G. Bennetts, V. A. Squire, D. Dumont, and L. Bertino (2012), Preliminary results from a two-dimensional model of wave-ice interactions in the Fram Strait, in *Proceedings of the Arctic Technology Conference*, vol. 2, pp. 1071–1078, OnePetro, Houston, Tex.
- Williams, T. D., L. G. Bennetts, D. Dumont, V. A. Squire, and L. Bertino (2013a), Wave-ice interactions in the marginal ice zone. Part 1: Theoretical foundations, *Ocean Model.*, *71*, 81–91.
- Williams, T. D., L. G. Bennetts, D. Dumont, V. A. Squire, and L. Bertino (2013b), Wave-ice interactions in the marginal ice zone. Part 2: Numerical implementation and sensitivity studies along 1D transects of the ocean surface, *Ocean Model.*, *71*, 92–101.
- Zhang, J., A. Schweiger, M. Steele, and H. Stern (2015), Sea ice floe distribution in the marginal ice zone: Theory and numerical experiments, *J. Geophys. Res.*, *120*, 3484–3498, doi:10.1002/2015JC010770.